CALLIBRATION PROCEDURE AND CHARACTERIZATION OF A COMMERCIAL MULTIPHOTON MICROSCOPE TO MEASURE POLARIZATION SECOND HARMONIC GENERATION MICROSCOPY

P. Garcia-Canadilla[2], I. Torre[2], M. Calvo[3], A. Gonzalez-Tendero[2], E. Gratacos[2], I. Amat-Roldan[1,2]

[1]TransMural Biotech, S.L., Barcelona, Spain
[2]Fetal and Perinatal Research Group, Departments of Maternal-Fetal Medicine and Neonatology, Institut Clinic de Ginecologia, Obstetrícia i Neonatologia, Hospital Clínic de Barcelona, IDIBAPS, Universitat de Barcelona, Centro de investigación Biomédica en Red de Enfermedades Raras, CIBER-ER, Instituto Salud Carlos III, Barcelona, Spain.
[3]Serveis Cientifico Tècnics, Facultad de Medicina, Universitat de Barcelona-IDIBAPS, Barcelona, Spain.

ABSTRACT

Polarization Second Harmonic Generation enables to quantify some of the underlying molecular details of key biological structures within muscle, axons and collagen at suboptical scales. However, it is only available in dedicated labs. In this work we detail a procedure to adapt and calibrate a commercial multiphoton microscope (Leica TCS-SP5) to acquire PSHG images reliably. For this, two different procedures were developed: (1) using inexpensive starch granules as polarization probe to estimate incident laser polarization within a region, and (2) using a fluorophore in solution to estimate the incident intensity arriving to each pixel of the image. This works might help to broaden the users of PSHG acquisition in microscopy as well as to provide the elements to correct for experimental errors.

Index Terms— Nonlinear optics, birefringence, biophotonics, calibration

1. INTRODUCTION

Second harmonic generation (SHG) is a promising microscopy technique for visualizing unstained structures with high resolution and contrast, such as collagen, myosin, microtubulin, amylopectin and cellulose. Some of these SHG-active structures play a major role in many biological problems [1]. SHG is a nonlinear optical process that occurs by interaction of ultrashort laser pulses with non-centrosymmetric materials. The inherent nonlinear optical properties are characterized by a $\chi^{(2)}$ tensor, which reflects some of the underlying molecular details of SHG-active structures at suboptical scales [2]. SHG shows polarization dependency and this physical mechanism has been used to generate contrast in many studies. Particularly, $\chi^{(2)}$ tensor can be solved in many interesting conditions for biomedical researchers. For this, a method based on acquiring a series of images at different linear polarization angles and subsequent fitting to a biophysical model that assumes a fiber-like structure was firstly proposed in 2002 [3]. This technique is referred as polarization SHG (PSHG) and has been used in axons, collagen fibers, C. elegans, muscle and cardiac cells and many others. In spite of all the advantages, commercial microscopy systems do not have dedicated hardware and software packages.

In this work we detail a procedure to adapt and calibrate a commercial multiphoton microscope (Leica TCS-SP5) to acquire PSHG images reliably. For this, two different procedures were developed: (1) using inexpensive starch granules as polarization probe to estimate incident laser polarization within a region, and (2) using a fluorophore in solution to estimate the incident intensity arriving to each pixel of the image. These two procedures will characterize important aspects of the polarization-sensitive microscope and set the uncertainty of the measurements in future experiments. Furthermore, the proposed recipe is cheap and fast to be performed in a commercial system once it has been programmed. Due to the fact that polarization is extremely dependent on optical path, the system becomes very sensitive to small alignment variations from different sources. For example, thermal expansion-relaxation suffered by the system due to temperature changes along the day, ground vibrations or even the standard utilization of the microscope by different users. Therefore it is always recommended to periodically align a microscope depending on the laboratory conditions. This work details a methodology that can be performed by a laboratory technician with automation of critical steps and simplifies this procedure to guarantee reproducibility and quality of the acquired images.

2. MATERIALS AND METHODS

2.1. Sample preparation

The developed procedure is composed by two steps: (1) starch granules diluted in water and sandwiched between two microscopy slides; (2) 8 µg/µl of fluorophore AlexaFluor® 488 (Molecular Probes; A-11001) diluted in distilled water and mounted on a glass slide.

2.2. Microscope modification

A commercial attenuation control from Leica based on a polarizator rotator and an analyzer was installed. Leica technicians removed the analyzer and proceed to the alignment of the system and calibration of the attenuator.

2.3. Starch as polarization probe

Starch has been previously used for measurement of ultrashort pulse width at the sample plane of a multiphoton microscope [4] because its natural nonlinear optical properties and efficient SHG. Furthermore, it is cheap, nontoxic, disposable and highly suitable for in-vivo experiments. As amylopectin, the SHG-active structures inside a starch granule are radially oriented [5], starch can be used as polarization probe [6]. An ideal starch granule can be modeled as a set of electric dipoles arranged radially (Fig. 1). When a starch granule is illuminated with an intense electric field at a certain polarization, only the parallel component of the electric field to the dipoles produce SHG. The efficiency is then proportional to the squared dot product between the dipole and the electric field. Thus, PSHG performed in a granule optically sliced at its equator shows a $\cos^2$ dependency of the SHG signal [6], which is characteristic of its radial structure.

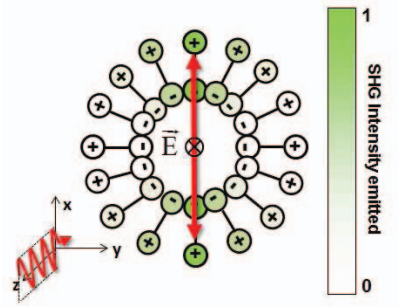


Figure 1. Physical model of starch granule architecture. Each dipole represents an amylopectin molecule. Electric field polarization direction is represented with the red arrow.

2.4. Acquisition of image sequences

Two parameters affecting the incident polarization can be controlled through Leica software and be programmed for automated acquisition: transmission control of optical intensity (*trans*) and image rotator (*rot*). These two parameters were scanned for imaging two objects: diluted starch granules in water and diluted fluorophore.

2.5. Developed software

2.5.1 Starch granule segmentation and center tracking

As starch granules were suspended in water, slight movement from granules appeared during image acquisition. In order to perform posterior processing correctly, it was necessary to estimate and correct the starch granule movement. For this, first granule's starch was automatically segmented by estimating the background gray level and binarizing, and a morphological closing was performed to remove small holes. Granule's perimeter was extracted and was smoothed for noise reduction. After that, center of mass was estimated frame by frame. Once the center of starch granule was computed, all images with different polarization angles from same experiment were corrected and added to check whether it fitted with the model (see Fig. 2).

2.5.2. Estimation of polarization angle in starch

Once center and radius of starch granule were estimated, for every image, 5 concentric circles were plotted inside starch granule and intensity profile from each circle was plot radially. Those intensity profiles were averaged in order to reduce the noise and correct intensity variations due to illumination differences in same starch granule. After that, signal was low pass band filtered as all information of interested is concentrated in low frequencies. As shown in Fig. 4 by filtering the signal in frequency domain all noise was practically removed. Finally, filtered signal was fitted with a parametric function $f(\theta) = \hat{A}\cos^2(\theta(trans, rot) - \hat{\phi}) + \hat{B}$, where $\theta(trans, rot)$ is the scanned axis of polarization that depend on the Leica controls *trans* and *rot*, $\hat{\phi}$ is the estimated average orientation for an image, $\hat{A}$ is the contribution of purely linear polarization and $\hat{B}$ is the amount of non-linearly polarized light (i.e. circular polarization or unpolarized light).

2.5.3. Computation of characteristic system curves

For each image we obtain three parameters $(\hat{\phi}, \hat{A}, \hat{B})$ that depend on *trans* and *rot*. Optimal values are those for which we minimize the $\hat{B}/\hat{A}$ ratio and allow accurate $\hat{\phi}$ sampling.

2.5.4. Characterization of intensity modulation

Relative variation of the delivered intensity at focal microscope at the different *trans* and *rot* conditions was done by averaging the total image intensity of 30 images of two-photon emission fluorescence of diluted Alexa fluor 488 and scanning *trans* and *rot* values. Characteristic curves are also calculated for the overall image although they can be computed at the pixel level (data not shown). Diluted fluorophore ensure no photobleaching at low average

intensities and results can be compared through time series. Root Mean Square Error (RMSE) was calculated for each rotator value and this can be used to evaluate whether such variations affect computations on the biophysical model.

3. RESULTS

3.1. Estimation of polarization angle in starch

Four different starch granules were studied at different image locations for different *trans* values and *rot* values. Results obtained for each starch granule were averaged and shown in Figs. 5-7.

3.1.1. Starch granule position tracking and segmentation
Example of the acquired image at a particular *trans* and *rot*, automated delineation and final image addition of all polarization are shown in Fig. 2A-C, respectively.

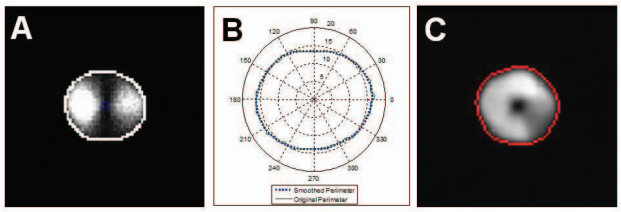


Figure 2. (a): Single image of starch granule at a given trans and rot values, perimeter of granule in white and center in blue. (b): Polar plot of starch granule perimeter, before (green) and after (blue) smoothing. (c): All polarizations centered and added, perimeter of granule in red.

Examples of the acquired images are shown in Fig.3A-C of the same granule at constant *trans* value of 30 and three *rot* values (0º, 45 and 90º) in which depth of modulation is clearly affected by the *rot* parameter.

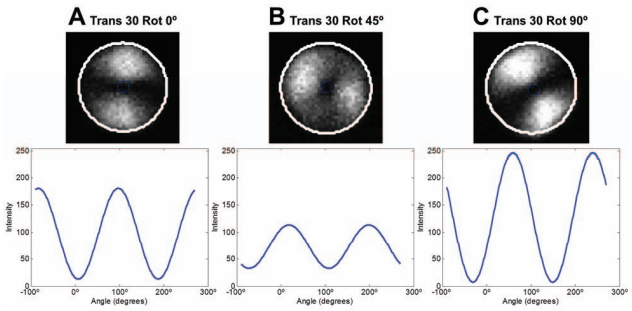


Figure 3. Examples of SHG imaging of a single starch granule at a constant *trans* value of 30, and *rot* value of (a) 0º, (b) 45º and (c) 90º.

3.1.2. Estimation of polarization angle in starch
Original and filtered angular intensity dependency with respect to the center can be seen in Fig.4A-B, respectively.

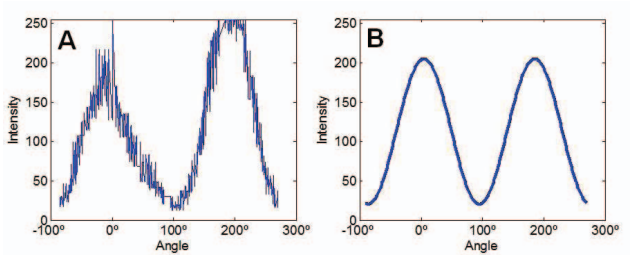


Figure 4. SHG intensity before (a) and after (b) filtering.

3.1.3. Computation of characteristic system curves
Results of $\hat{\phi}(trans, rot)$ for the scanned controls and averaging of the four granules is shown in Fig.5.

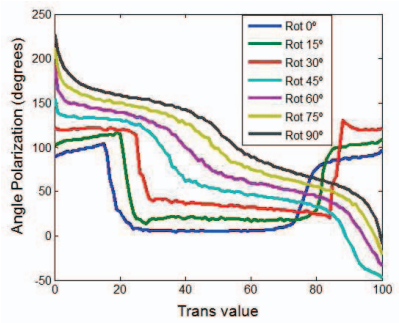


Figure 5. Polarization angle estimation (in degrees) plotted versus trans value for different rotator positions. The resulting graph is the average of four different starch granules.

Results of $\hat{B}/\hat{A}$ as a function of *trans* and *rot* are shown in Fig. 6. The lowest average $\hat{B}/\hat{A}$ values were obtained for rotator position 90º although the best acquisitions might be obtained by acquiring polarization data at different pairs of *rot* and *trans*.

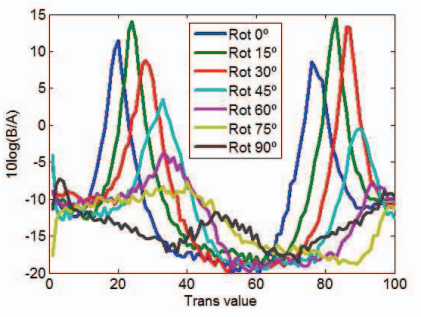


Figure 6. $\hat{B}/\hat{A}$ ratio in logarithmic scale for different *rot* values.

3.1.4. Characterization of intensity modulation.
Mean intensity value of each averaged image was calculated for each *trans* value and for the different rotator positions also. Intensity variation according to *trans* parameter was estimating and RMSE was calculated. As shown in Fig. 7 and Table 1, minimum RMSE was obtained for rotator position in 90º.

Rotator position	RMSE
0º	10,17%
15º	8,61%
30º	7,86%
45º	8,08%
60º	7,80%
75º	6,95%
90º	5,76%

Table 1. RMSE of intensity for different *rot* values.

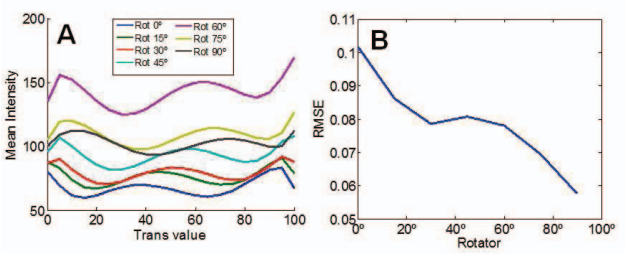


Figure 7. (a) The intensity variation according to *trans* parameter for each rotator position is shown; (b) average RMSE is calculated for each rotator position.

4. DISCUSSION

Analysis of the measured curves shows that the optimal conditions are achieved at *rot* of 90º, as both average $\hat{B}/\hat{A}$ ratio and RMSE of the intensity modulation along the changes of *trans* is minimum. Remarkably at *rot*=90º, additionally, the dynamic range of achievable is one of the broadest (Fig. 5) and very smooth along all the *trans* range which suggests that its accuracy is maximal. In order to perform, PSHG measurements it is required to perform at least two measurements at different linearly polarized angles within 0º and 180º (although a minimum of 6 is strongly recommended when the composition of the specimen is unknown and 9 sampling points are used in the literature). Additionally, Fig. 5 provides the relation of the incident polarization angle and the *trans* value. Therefore, a program with fix rot of 90º and variable *trans* was introduced in a programmed acquisition to introduce into the Leica software a standard protocol for PSHG imaging with 9 sampling points at 0, 20, 40, 60, 80, 100, 120, 150, 160 degrees of linear polarization. Furthermore, the information of the non-linearly polarized part of the electric field (B/A ratio) and the intensity modulation of different *trans* at a given *rot* value (fluorophore measurements) will allow to correct for the PSHG signal detected in specimen signal and reduce the experimental errors when fitting the biophysical model.

5. CONCLUSIONS

In this paper we have shown that is possible the acquisition of PSHG images in a commercial multiphoton microscope by adding one commercial piece of hardware (attenuation control based on polarization) from the same brand and proper calibration procedure, which was done by the authorized technical service of the microscope. We have automated this procedure and developed a software package in order to check and correct for potential misalignments occurring in the system. This methodology will also enable us to evaluate and trace the misalignment of the system reliably. The optimal results obtained for our microscope might not be directly transferable to other microscopes of the same brand and model as small variations in the installation might produce changes of orientation of polarization. Therefore, it is recommended to follow the proposed procedure to find specific optimal values. Furthermore, the characterization of the polarization state of the light beam at the focal plane will help to reduce experimental variability when fitting the known biophysical models into data, which might improve the reliability of the method and understanding of the reported measurements.

This works helps to broaden the users of PSHG acquisition in microscopy, as it is an emerging technique with high potential applications in many biomedical fields.

5. REFERENCES

[1] Campagnola P. J. and Loew L. M., "Second-harmonic imaging microscopy for visualizing biomolecular arrays in cells, tissues and organisms," *Nature Biotechnol,* 21, 1356-60, 2003.

[2] Chu S. W., Chen S. Y., Chern G. W., Tsai T. H., Chen Y. C., Lin B. L. and Sun C. K., "Studies of $\chi^{(2)}/\chi^{(3)}$ tensors in submicron-scaled bio-tissues by polarization harmonica optical microscopy," *Biophys. J.,* 86 3914-22, 2004.

[3] Stoller P., Reiser K. M., Celliers P. M., and Rubenchik A. M., "Polarization-modulated second harmonic generation in collagen," *Biophys. J.* 82(6), 3330–3342, 2002.

[4] Amat-Roldan I., Cormack I.G., Loza-Alvarez P., Artigas D., "Starch-based second-harmonic-generated collinear frequency-resolved optical gating pulse characterization at the focal plane of a high-numerical-aperture lens," *Opt. Lett*. 29, 2282-2284, 2004.

[5] Gallant, D.J., Bouchet, B., Baldwin, P.M., 1997. "Microscopy of starch: evidence of a new level of granule organization," *Carbohydrate Polymers* 32, 177–19, 1997.

[6] Psilodimitrakopoulos S., Santos S., Amat-Roldan I., Mathew M., Thayil A. K. N, Artigas D. and Loza-Alvarez P., "Polarization dependant in vivo second harmonic generation imaging of Caenorhabditis elegans vulval, pharynx and body wall muscles," *Proceedings of the SPIE*, 686008, 2008.

6. ACKNOWLODGEMENTS

Patricia Garcia-Canadilla and Transmural Biotech acknowledge the cvRemod project under the CENIT 20092012 programme of the industrial and technological development center (CDTI). All authors acknowledge Servei Tecnic de la Universitat de Barcelona, Luis Enciso from the Maternal-Fetal Medicine team of Hospital Clinic de Barcelona, Leica Microsystems Advanced Fluorescence Systems team of Spain, and particularly, Olga Sánchez, Joan L. Monteagudo and Mark Munro for their collaboration and help.